JOURNAL OF MATERIALS SCIENCE 31 (1996) 1243–1254

Porosity formation in Al–9 wt% Si–3 wt% Cu–X alloy systems: measurements of porosity

N. ROY, L. ZHANG, P. R. LOUCHEZ, F. H. SAMUEL
Département des Sciences Appliquées, Université du Québec à Chicoutimi, Chicoutimi (Québec), Canada, G7H 2B1

A set of 72 experiments was carried out to study the effects of solidification conditions, hydrogen content and additives on the formation of porosity in Al–9 wt% Si–3 wt% Cu–X alloy systems. It was found that not all alloying elements contribute to porosity formation in the Al–Si–Cu base system. Some of these elements, e.g. magnesium, titanium and phosphorus, tend to reduce both pore size and density. Hydrogen is the strongest element that induces porosity formation, its effect being reinforced either by the addition of strontium or by increasing the solidification time, or both. Grain refining is found to reduce pore density and pore size, and results in a fine dispersion of the pores throughout the alloy matrix. The necessary precautions to be taken in measuring the porosity in these alloys are reviewed in this paper. Accurate measurements of porosity using image analysis need careful adjustment of optical parameters, namely focus, illumination and grey level, as well as a careful selection of the number of field measurements required to represent correctly the sample surface.

1. Introduction

One of the biggest problems in aluminium castings is porosity, primarily caused by turbulent transfers during pouring of the molten metal. Apart from affecting the surface finish, porosity, in particular hydrogen-induced porosity, is always a cause for concern because it is detrimental to the mechanical properties.

The formation of porosity in solidifying metals can be attributed mainly to two effects: shrinkage, resulting from the volume decrease accompanying solidification, and the evolution of dissolved gases, resulting from the decrease in solubility of these gases in the solid as compared to the liquid metal [1–11]. These effects may manifest themselves separately or, as is more often the case, simultaneously, interacting with each other to develop the resulting porosity observed. On account of this, it is difficult, in most casting situations, to state which factor is predominant in causing the porosity. Precipitation of hydrogen in the solid state is also a third possible cause [1, 3].

A vast amount of theoretical work as well as various experimental studies investigating the phenomenon of porosity have been reported in the literature [2–15]. Different types of porosity have been observed, mechanisms of pore formation suggested and models developed to substantiate them.

The present work covers the results of a study carried out to determine the role of solidification parameters, hydrogen content, alloying elements and additives on porosity formation in Al–9 wt % Si–3 wt % Cu–*X* alloy systems. This article focuses on the parameters that affect the accuracy of porosity measurements, in particular those made employing image analysis. Metallographic aspects of the work and the effect of the different parameters on porosity formation will be dealt with in comprehensive detail in a forthcoming article. This study is part of an extensive ongoing research programme covering the different factors involved in the production of quality aluminum automotive alloy castings.

2. Experimental procedure

Aluminium alloys containing 9 wt % Si – 3 wt % Cu–0.15 wt % Fe were prepared from pure elements and supplied in the form of 12.5 kg ingots. Table I lists the desired chemical compositions of the alloys used in the present study. The compositions were adjusted by adding alloying elements or additives using aluminium binary master alloys. Table II lists the final compositions of the alloys, as obtained from inductive couple plasma (ICP) analysis. In Table I, the alloys are classified into three main groups: f, h and s alloys, corresponding to a group of iron (Fe), a group of hydrogen (H), and a group of strontium (S), respectively.

The alloys were melted in a silicon carbide crucible of 7 kg capacity using an electrical resistance furnace. The melting temperature was adjusted at 735 ± 5 °C. Two tapered wedge steel moulds were employed, one at an opening angle of 5° and heated at 40 °C, the second at an opening angle of 30° and heated at 300 °C. The schematic diagrams of these moulds are shown in Fig. 1a, b, respectively. Prior to pouring, the mould was inclined at 35° with respect to the vertical axis, and moved up slowly during pouring.

0022–2461

TABLE I Aimed compositions (wt %) and hydrogen levels (ml $100\,g^{-1}$ Al) for the alloys prepared for the present work

Alloy	Zn	Fe	Mg	Mn	Ti	Sr	P	GR[a] (Ti)	H	Si	Cu
f1	0	0.1		0.0			0				
f2	0	0.1		0.6			0.006				
f3	0	1.0		0.0			0.006				
f4	0	1.0	0.35	0.6	0.13	0.015	0	0.02	0.25		
f5	3	0.1		0.0			0.006				
f6	3	0.1		0.6			0				
f7	3	1.0		0.0			0				
f8	3	1.0		0.6			0.006				
h1			0				0	0.00	0.1	9	3
h2			0				0	0.02	0.4		
h3			0				0.006	0.00	0.4		
h4	1.5	0.55	0	0.3	0.13	0.015	0.006	0.02	0.1		
h5			0.7				0	0.00	0.4		
h6			0.7				0	0.02	0.1		
h7			0.7				0.006	0.00	0.1		
h8			0.7				0.006	0.02	0.4		
s1	0		0		0.00	0.000					
s2	0		0		0.25	0.030					
s3	0		0.7		0.00	0.030					
s4	0	0.55	0.7	0.3	0.25	0.000	0.003	0.02	0.25		
s5	3		0		0.00	0.030					
s6	3		0		0.25	0.000					
s7	3		0.7		0.00	0.000					
s8	3		0.7		0.25	0.030					

[a] GR, grain refiner (Al–5 wt % Ti–1 wt % B).

TABLE II Actual compositions of the cast alloys (wt %) used in the present work (obtained from ICP analysis)

Alloy	Si	Cu	Zn	Fe	Mg	Mn	Ti	Sr	P
f1		3.08	0.01	0.22	0.32	0.00	0.140	0.013	0.0000
f2		3.18	0.01	0.16	0.35	0.60	0.150	0.023	0.0019
f3		3.19	0.10	1.19	0.31	0.00	0.150	0.090	0.0000
f4		3.31	0.06	1.06	0.33	0.62	0.140	0.022	0.0000
f5		3.23	0.70	0.19	0.29	0.00	0.137	0.012	0.0033
f6		2.77	0.70	0.19	0.28	0.06	0.148	0.014	0.0000
f7		2.78	0.80	1.00	0.28	0.00	0.110	0.014	0.0000
f8		2.94	1.13	0.95	0.27	0.60	0.140	0.015	–
h1		3.02	1.48	0.54	0.08	0.35	0.130	0.024	0.0000
h2		3.32	1.51	0.60	0.09	0.20	0.190	0.022	0.0000
h3		3.06	1.49	0.55	0.08	0.30	0.130	0.017	0.0030
h4		3.05	1.47	0.55	0.08	0.28	0.140	0.017	0.0033
h5		2.98	1.50	0.55	0.66	0.29	0.130	0.024	–
h6	8.93	3.41	1.56	0.57	0.77	0.26	0.190	0.024	0.0000
h7		3.68	1.56	0.57	0.61	0.36	0.140	0.017	0.0037
h8		3.12	1.47	0.53	0.66	0.30	0.190	0.027	0.0011
s1		3.40	0.00	0.57	0.02	0.30	0.040	0.002	0.0020
s2		3.16	0.00	0.56	0.01	0.30	0.270	0.043	0.0025
s3		3.06	0.00	0.43	0.33	0.31	0.050	0.042	0.0025
s4		3.35	0.00	0.53	0.24	0.30	0.290	< 0.002	0.0025
s5		2.84	1.80	0.56	0.01	0.31	0.030	0.030	0.0025
s6		2.90	1.90	0.79	0.01	0.31	0.090	< 0.002	0.0025
s7		3.16	1.70	0.54	0.67	0.30	0.030	< 0.002	0.0025
s8		2.87	1.80	0.97	0.30	0.30	0.060	0.038	0.0025

The Alscan™ unit is one of the commercial techniques available for direct measurement of the melt hydrogen content. The melt temperature is measured simultaneously. In the present work, the melt hydrogen level was monitored using an Alscan™ unit. In addition, specimens were also cast simultaneously in Ransley moulds (for each pouring/casting) from which "Ransley" samples were machined for determination of the hydrogen content using the Leco subfusion technique. This is one of the standard methods for obtaining accurate analysis of the hydrogen content in a melt [16]. For each pouring, specimens for chemical analysis were also taken. Table III lists the hydrogen contents obtained from Leco analysis of the alloy samples.

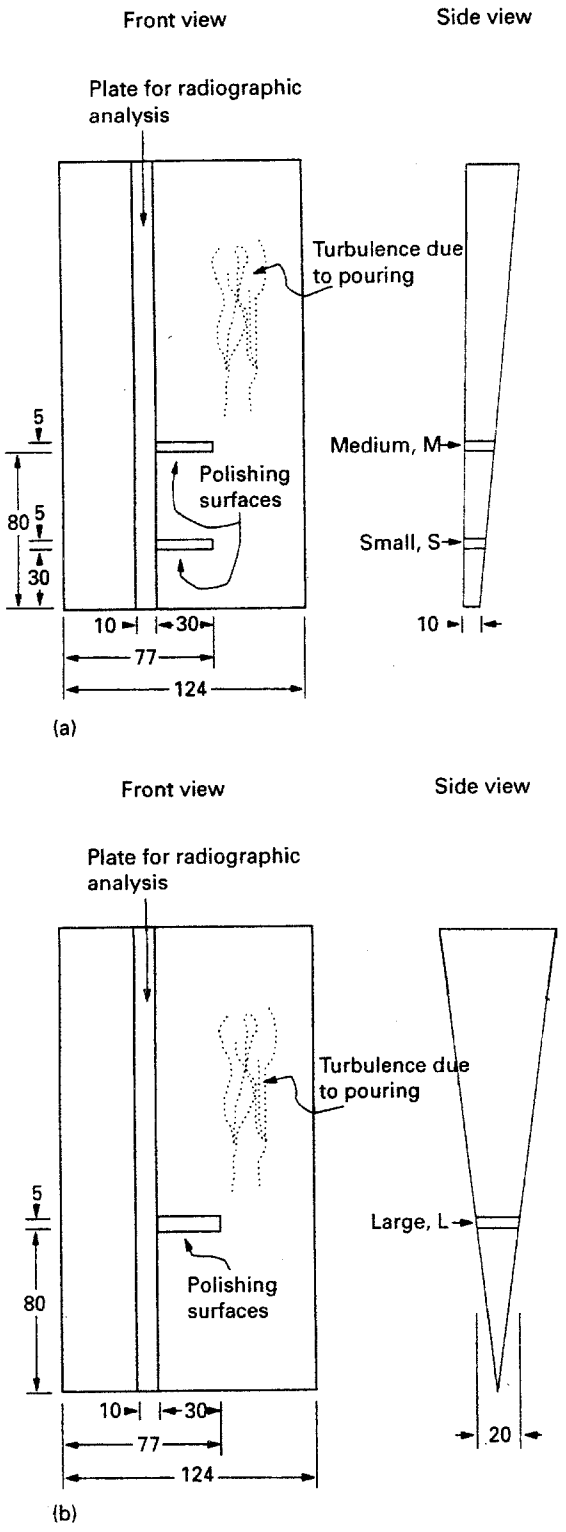

Figure 1 Schematic diagram of (a) cold mould, and (b) hot mould (all dimensions in mm).

3. Results and discussion

3.1. Thermal analysis

Three pairs of thermocouples (Chromel–Alumel, type K), were each placed in the two moulds at positions from which samples for metallographic observations were prepared. Each pair consisted of two thermocouples separated by a 5 mm distance. Fig. 2a–c shows the temperature–time curves obtained from small (S), medium (M) and large (L) samples, respectively, taken from the positions shown in Fig. 1. In all three cases, the arrest corresponding to the $(Al + Al_2Cu)$ eutectic reaction could not be resolved under the directional solidification conditions of the study, when the solidification front is normal to the eutectic growth direction [17]. Based on earlier thermal analysis work on 380 alloy [18], the solidus temperature was taken to be 500 °C. Table IV summarizes the data obtained from Fig. 2.

TABLE III Hydrogen measurements (ml $100\,g^{-1}$ Al)

Alloy	H2
f1	0.22
f2	0.25
f3	0.20
f5	0.25
f6	0.31
f7	0.31
f8	0.25
h1	0.06
h2	0.52
h3	0.49
h4	0.13
h5	0.57
h6	0.12
h7	0.13
h8	0.45
s1	0.28
s2	0.24
s4	0.23
s5	0.26
s6	0.21
s7	0.21
s8	0.29

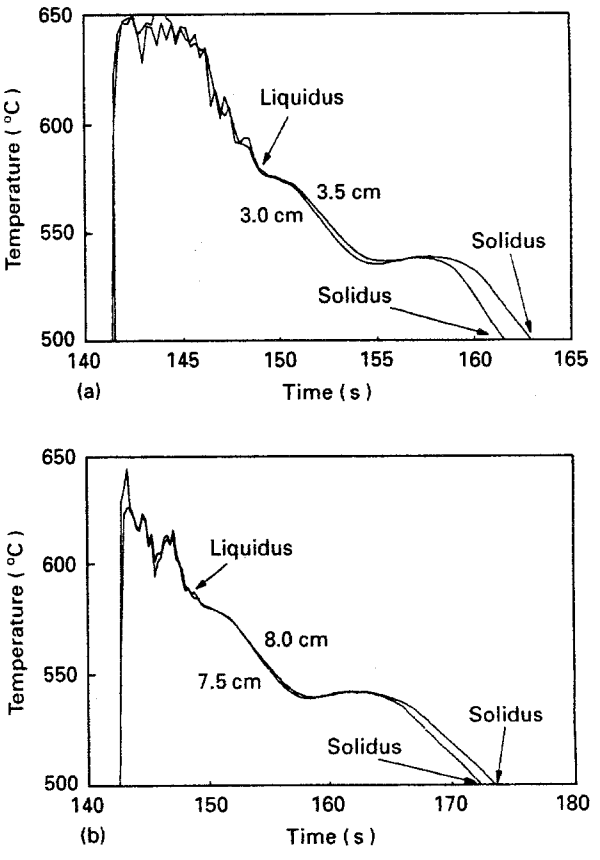

Figure 2 Temperature–time curves for (a) small, (b) medium, and (c) large samples.

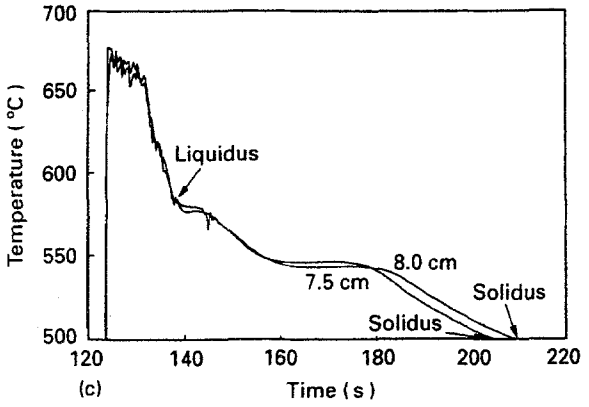

Figure 2 Continued.

TABLE IV Solidification parameters

Specimen	Thermocouple position (cm)[a]	Solidification time, t_s (s)	Solidus velocity, V_s (cm s^{-1})
Small (S)	3.0	12.5	0.450
	3.5		
Medium (M)	8.0	25.2	0.360
	7.5		
Large (L)	8.0	70.9	0.114
	7.5		

[a] Height as measured from the bottom of the mould.

3.2. Image analysis

As shown in Fig. 1, three samples termed small (S), medium (M) and large (L) were cut from each casting, and their upper surfaces polished for measurements of porosity. The porosity was quantified using a Leco 2001 image analyser, in conjunction with an optical microscope (Olympus PMG3). The accuracy of pore size and pore density measurements using image analysis depends on four parameters: focus, illumination, grey level and the number of images analysed per sample.

Focus is one of the most important parameters for precise determination of pore shape and size. All images were measured at a magnification of × 50. Each image, however, was first adjusted at × 500 (the focusing being very sensitive at such high magnification), before switching to × 50. The microscope employed in the present investigations is provided with a fine focus knob that is graduated into 200 divisions. With respect to the latter, and at × 50, the image was under focused between 0 and 40 divisions, well focused between 60 and 120 divisions, and over focused between 140 and 200 divisions, respectively. On changing the magnification from × 500 to × 50, a final focusing of about ± 10 divisions was required. Fig. 3a–c shows the dependence of measurements on focusing.

Illumination is another important factor to be considered in precise measurements of porosity. When the illumination is too high, the image analyser monitor screen tends to become magenta coloured (a deep purplish red). The intensity of illumination was therefore controlled in such a way that only one magenta spot was seen on the screen. Fig. 4a–c exemplifies the variation in number of pores, pore length and

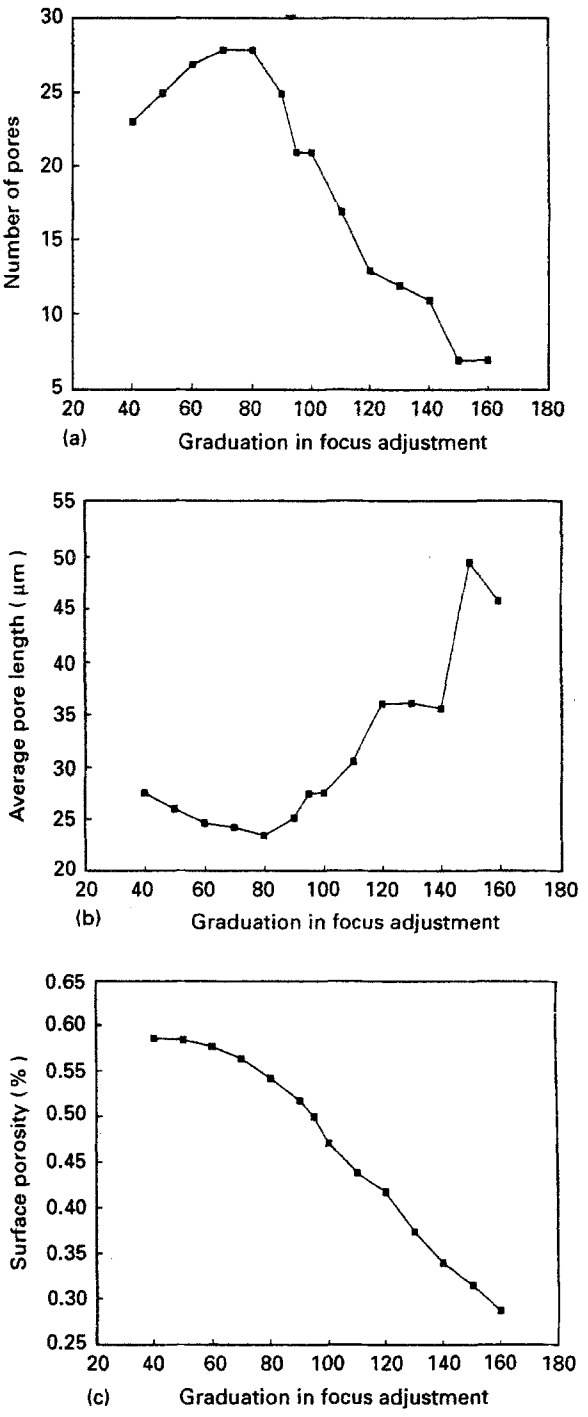

Figure 3 Dependence of (a) number of pores, (b) average pore length, and (c) per cent surface porosity on the adjustment of focus.

per cent of surface porosity (about 0.85% the porosity volume fraction) with intensity of illumination. As can be seen, measurements are unreliable when the illumination is either low (dark screen) or high (magenta screen).

The grey level for the Leco 2001 image analyser ranges between 0 and 225, 0 corresponding to black, and 225 to white. The grey level was adjusted in such a way that all pores were saturated, i.e. having the same colour. This adjustment was made only once prior to carrying out all measurements (72 specimens measured in total).

The last parameter that requires attention is the number of images needed to produce reliable data. As shown in Fig. 1a, the dimensions of the small sample

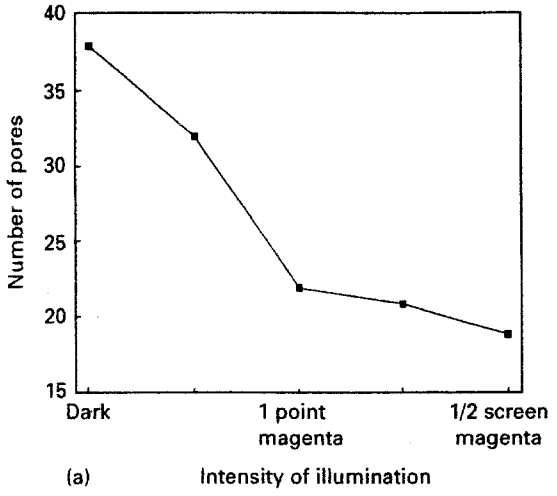

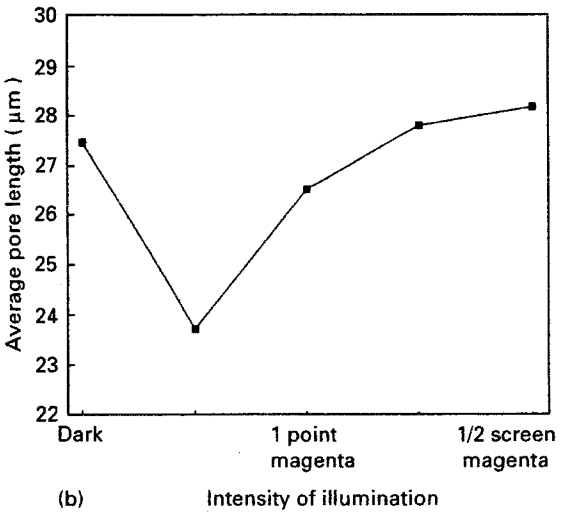

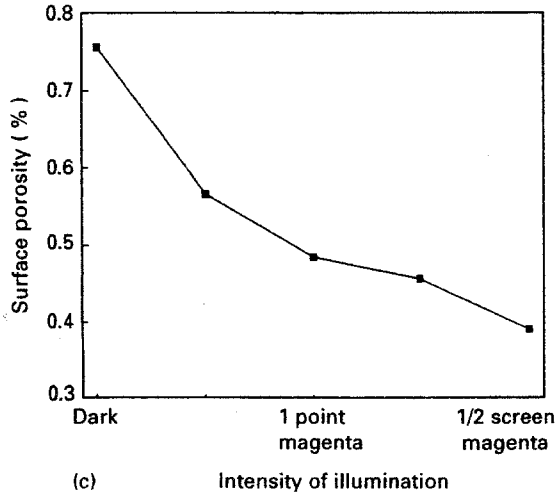

Figure 4 Dependence of (a) number of pores, (b) average pore length, and (c) per cent surface porosity on light intensity.

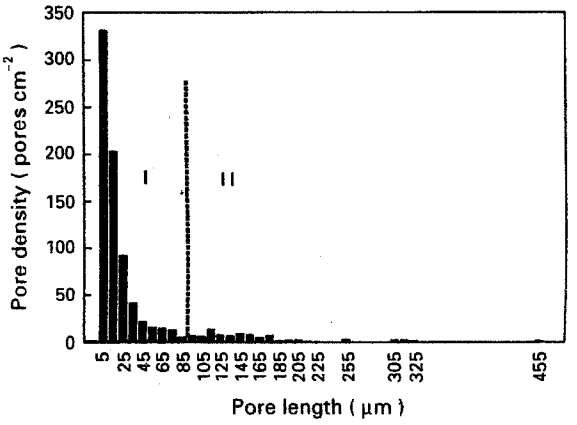

Figure 5 A typical pore distribution curve.

TABLE V Results of eight porosity measurements made on the s2S specimen

Measurements no.	1	2	3	4	5	6	7	8
All pores								
Surface porosity (%)	0.38	0.35	0.34	0.34	0.34	0.32	0.33	0.33
Exponential part of pore density versus pore length distribution curve								
Density, pores cm^{-2}	272	250	282	236	240	259	245	196
Limiting length, μm	106	87	77	84	93	87	87	87
Average length, μm	25.2	21.3	16.8	21.4	23.2	21.6	21.1	21.6
Standard deviation	25	21.1	17	21.5	23.3	21.6	21.3	21.5
Irregular part of pore density versus pore length distribution curve								
Density, pores cm^{-2}	29	37	45	37	33	35	36	38
Maximum length, μm	196	193	193	193	196	180	193	193
Average length, μm	139	127	119	125	130	126	127	125
Standard deviation	24	27	30	27	26	25	26	27
Exponential part of pore density versus pore area distribution curve								
Density, pores cm^{-2}	207	204	232	186	185	208	198	154
Limiting area, μm^2	300	300	227	269	289	289	289	300
Average area, μm^2	69	69	49	63	66	66	65	62
Standard deviation	68	69	49	63	67	67	66	63
Irregular part of pore density versus pore area distribution curve								
Density, pores cm^{-2}	94	83	94	87	87	86	83	80
Maximum area, × 1000 μm^2	20.6	20.3	20.3	19.8	20.2	18.8	20.2	20.3
Average area, μm^2	3842	4002	3505	3765	3771	3512	3852	4025
Standard deviation	4294	4198	4116	4085	4146	3632	4235	4241

TABLE VI Statistical parameters based on the eight porosity measurements made on the s2S specimen

Statistical parameter	Average, μ	Standard deviation, σ	Precision, % σ/μ
All pores			
Surface porosity (%)	0.341	0.018	5
Exponential part of pore length distribution curve			
Density, pores cm^{-2}	248	24.4	10
Limiting length, μm	88	7.8	9
Average length, μm	21.5	2.2	10
Standard deviation	21.5	2.2	10
Irregular part of pore length distribution curve			
Density, pores cm^{-2}	36	4.3	12
Maximum length, μm	192	4.8	2
Average length, μm	127	5.3	4
Standard deviation	26	1.7	6
Exponential part of pore area distribution curve			
Density, pores cm^{-2}	197	21	11
Limiting area, μm^2	283	23	8
Average area, μm^2	64	6.1	10
Standard deviation	64	6.1	10
Irregular part of pore area distribution curve			
Density, pores cm^{-2}	87	4.7	5
Maximum area, $\times 1000\ \mu m^2$	20	0.5	3
Average area, μm^2	3784	182	5
Standard deviation	4118	195	5

TABLE VII Percentage surface porosity for small (S)[a] and large (L)[b] samples

Alloy sample	Surface porosity (%)
f1S	0.451
f1L	1.160
f2S	0.236
f2L	0.444
f3S	0.068
f3L	0.269
f4S	0.152
f4L	0.513
f5S	0.280
f5L	0.813
f6S	0.611
f6L	1.506
f7S	0.207
f7L	0.730
f8S	0.260
f8L	0.396
h1S	0.064
h1L	0.094
h2S	1.990
h2L	2.433
h3S	2.250
h3L	3.066
h4S	0.044
h4L	0.065
h5S	1.830
h5L	2.835
h6S	0.145
h6L	0.218
h7S	0.032
h7L	0.114
h8S	1.804
h8L	2.522
s1S	0.061
s1L	0.680
s2S	0.366
s2L	1.308
s3S	0.0210
s3L	0.2466
s4S	0.062
s4L	0.282
s5S	0.358
s5L	1.285
s6S	0.042
s6L	0.624
s7S	0.110
s7L	0.675
s8S	0.060
s8L	0.389

[a] S = $t_s \sim 12.5$ s.
[b] L = $t_s \sim 71$ s.

are 1 × 3 cm. For such a sample, the number of fields needed to cover the entire surface are six (rows) × 16 (images per row) at a magnification of × 50. Since the sample was in direct contact with the inner surfaces of the mould, the cooling rate at its periphery would be much higher than that near the centre. For this reason, image readings from the outer edges were discarded. The number of fields then required to scan the rest of the sample was four (rows) × 14 (images per row). In selecting the field of view, precautions were taken at all times to avoid cutting-off of any pores. A similar procedure was followed for the medium and large samples.

Fig. 5 shows a typical pore distribution curve obtained from an s2S alloy sample. It consists of two parts: an exponential part comprising small pores (marked I), and an irregular part representing large pores (marked II). The two parts are separated by a limiting value. For an appropriate evaluation of the consistency of measurements made following the abovementioned procedure, the porosity in the s2S sample was measured eight times. The results are shown in Table V. Based on these measurements and the associated standard deviation, the precision of the measurements could be evaluated as shown in Table VI. As can be noted, errors in measuring the exponential parameters (small pores) are of the order of 10%. For the large pores, the errors drop to about 5%.

Tables VII–X summarize the variation in porosity parameters for small and large samples covering the entire solidification range employed in the present investigation. Taking into consideration the alloying elements, additives and hydrogen levels present in each alloy/sample, the following observations were made.

1. For a given hydrogen level, not all alloying elements necessarily contributed to porosity formation. In fact, a number of these elements showed an opposite effect, for example, magnesium, titanium and phosphorus.

2. Hydrogen was the strongest factor related to porosity formation, followed by strontium (added as Al–10 wt % Sr master alloy). Grain refining (through the addition of Al–5 wt % Ti–1 wt % B) reduced both per cent of

TABLE VIII Average and maximum pore areas for small (S) and large (L) samples

Alloy sample	Pore density versus pore area distribution curve			
	Exponential part		Irregular part	
	Average area (μm^2)	Maximum area (μm^2)	Average area (μm^2)	Maximum area (μm^2)
f1S	54.00	258.0	4902.0	22601.0
f1L	74.75	305.0	15913.0	57630.0
f2S	66.00	258.0	4666.0	142348.0
f2L	67.00	321.0	8988.0	105665.0
f3S	54.00	271.0	741.0	3465.0
f3L	72.00	341.0	1963.0	27501.5
f4S	64.00	291.0	1213.0	11061.0
f4L	58.00	248.0	4245.5	101841.5
f5S	67.00	248.0	3085.0	35277.0
f5L	99.00	434.0	6753.0	83270.0
f6S	50.00	250.0	7200.0	48148.0
f6L	64.00	281.0	13837.0	69324.0
f7S	66.40	300.0	1581.0	24958.0
f7L	70.00	316.0	3747.5	85184.5
f8S	55.00	769.0	2093.0	32216.0
f8L	81.00	352.0	2831.0	27099.5
h1S	65.00	271.0	972.0	6087.0
h1L	85.50	354.0	1525.0	7851.5
h2S	52.00	219.0	8781.0	83819.0
h2L	66.50	343.0	23991.5	397341.5
h3S	58.00	248.0	15847.0	83911.0
h3L	62.00	259.5	43615.0	153917.0
h4S	50.50	248.0	644.0	3588.0
h4L	63.50	284.0	1449.0	26390.0
h5S	66.00	271.0	13522.0	105494.0
h5L	63.00	310.0	25369.5	50471.5
h6S	59.50	248.0	1218.0	11704.0
h6L	73.00	321.0	1796.0	45827.5
h7S	49.50	250.0	486.0	1821.0
h7L	61.00	331.0	921.0	5556.0
h8S	57.50	269.0	7837.0	45750.0
h8L	57.50	281.0	15186.0	39448.9
s1S	83.00	321.0	2620.0	23170.0
s1L	120.00	286.0	9860.0	58302.0
s2S	64.00	283.0	3784.0	20042.0
s2L	75.00	341.0	14406.0	69706.0
s3S	42.00	196.0	507.0	2512.0
s3L	98.00	364.0	2169.0	29277.0
s4S	78.50	331.0	2497.0	26458.0
s4L	67.50	305.0	4011.0	26168.0
s5S	63.00	279.0	3178.0	26561.0
s5L	66.50	469.0	8352.0	89648.5
s6S	67.00	248.0	2320.0	13399.0
s6L	106.50	429.0	6813.5	217915.5
s7S	58.00	227.0	1515.0	18011.0
s7L	89.50	372.0	4191.5	12790.4
s8S	52.00	239.0	918.0	5036.0
s8L	70.00	290.2	2679.0	48989.0

TABLE IX Average and maximum pore lengths for small (S) and large (L) samples

Alloy sample	Pore density versus pore length distribution curve			
	Exponential part		Irregular part	
	Average length (μm)	Maximum length (μm)	Average length (μm)	Maximum length (μm)
f1S	16.70	73.9	122.0	209.0
f1L	22.07	98.3	185.5	376.5
f2S	18.80	86.8	150.0	598.0
f2L	18.62	104.5	198.5	619.0
f3S	15.20	103.0	135.0	135.0
f3L	17.75	116.0	181.0	278.0
f4S	18.70	106.0	137.0	203.0
f4L	18.80	115.0	213.0	657.5
f5S	21.60	90.0	143.0	286.0
f5L	24.75	129.0	175.5	522.6
f6S	16.80	83.9	154.0	323.0
f6L	18.50	103.0	215.5	437.0
f7S	20.40	100.0	157.0	296.0
f7L	18.76	113.0	195.0	627.0
f8S	15.60	103.0	158.0	367.0
f8L	21.70	119.0	169.0	283.0
h1S	19.20	123.0	173.0	184.0
h1L	18.10	110.0	188.0	248.0
h2S	21.60	90.3	175.0	458.0
h2L	19.85	98.3	216.0	371.0
h3S	21.10	93.3	229.0	431.0
h3L	16.95	107.7	321.0	675.0
h4S	14.40	103.0	–	–
h4L	17.00	109.5	183.0	424.0
h5S	18.60	106.0	224.0	468.0
h5L	17.75	119.0	357.0	691.0
h6S	17.90	113.0	147.0	199.0
h6L	18.85	120.5	219.0	527.0
h7S	12.90	87.1	–	–
h7L	16.75	98.3	129.0	213.0
h8S	19.90	93.3	175.0	386.0
h8L	18.05	105.0	247.0	703.0
s1S	27.30	113.0	179.0	235.0
s1L	29.20	146.5	245.0	338.0
s2S	21.50	88.5	127.0	192.0
s2L	21.30	119.0	217.0	408.0
s3S	12.90	90.0	–	–
s3L	26.70	171.0	198.5	373.0
s4S	19.70	116.0	215.0	215.0
s4L	19.00	99.8	159.0	399.0
s5S	22.50	103.0	158.0	273.0
s5L	24.50	103.0	185.0	454.5
s6S	24.50	113.0	141.0	141.0
s6L	26.35	169.0	290.0	344.0
s7S	19.00	100.0	173.0	350.0
s7L	21.80	154.0	217.0	514.0
s8S	15.70	90.3	144.0	200.0
s8L	20.80	123.0	182.0	395.0

surface porosity and pore size. It resulted, however, in a more uniform distribution of pores (see also [19, 20]).

3. Increasing the local solidification time or reducing the solidus velocity increased both the pore size and per cent of surface porosity.

3.3. Radiographic and microstructural evaluation

Plates for radiographic examination were cut as shown schematically in Fig. 1. Both surfaces were polished prior to testing. The main observations are summarized in Table XIa–c for the three groups, i.e. Fe, H and Sr, respectively. The symbols c and h indicate a cold or a hot mould, respectively.

The effect of increasing the hydrogen content from 0.06 to 0.57 ml $100\,g^{-1}$ Al on enhancing porosity formation is exemplified in Fig. 6. Grain refining (measured as 0.02 wt % Ti) resulted in small, well dispersed pores even at low cooling rates (employing a mould coated with refractory material and heated at 300 °C), Fig. 7. As seen in Tables II and III, the

TABLE X Pore density (number of pores cm^{-2}) for small (S) and large (L) samples

Alloy sample	Pore density–pore length distribution curve		Pore density–pore area distribution curve	
	Exponential part	Irregular part	Exponential part	Irregular part
f1S	213.0	58.40	101.0	90.10
f1L	239.5	68.10	199.1	108.40
f2S	208.0	11.30	171.1	48.10
f2L	372.0	23.05	315.0	79.55
f3S	575.0	1.00	469.0	57.30
f3L	842.5	11.25	746.0	108.00
f4S	552.0	10.20	461.0	101.00
f4L	601.0	30.70	493.0	138.00
f5S	295.0	22.50	231.0	86.00
f5L	414.5	50.70	344.0	121.50
f6S	173.0	52.20	141.0	83.90
f6L	244.0	57.85	206.0	96.50
f7S	534.0	14.30	436.0	113.00
f7L	787.0	39.00	644.0	179.00
f8S	794.0	18.40	707.0	105.00
f8L	648.0	76.10	540.0	134.00
h1S	271.0	2.00	225.0	48.10
h1L	182.0	10.20	176.0	31.75
h2S	641.0	173.00	476.0	33.00
h3L	388.5	116.50	327.0	178.00
h3S	255.0	86.00	203.0	138.00
h3L	245.0	57.85	210.0	91.75
h4S	362.0	–	319.0	43.00
h4L	363.0	9.20	319.5	48.10
h5S	422.0	63.50	351.0	134.00
h5L	490.5	56.30	421.0	126.00
h6S	539.0	10.20	453.0	97.30
h6L	544.5	14.30	473.5	78.30
h7S	340.0	–	305.0	34.80
h7L	555.0	16.40	495.0	85.00
h8S	488.0	135.00	396.0	227.00
h8L	492.5	127.50	414.0	167.00
s1S	65.0	2.30	45.5	21.90
s1L	346.5	26.60	265.5	107.35
s2S	247.0	36.20	197.0	86.70
s2L	390.0	72.15	326.0	136.50
s3S	193.0	–	166.0	27.60
s3L	358.5	10.50	288.5	82.50
s4S	128.0	1.00	107.0	21.50
s4L	429.0	24.60	377.0	76.80
s5S	336.0	26.60	255.0	107.00
s5L	303.5	65.00	231.0	137.50
s6S	69.6	1.00	54.3	16.40
s6L	328.6	30.00	265.0	92.00
s7S	762.0	7.20	205.0	64.50
s7L	636.5	22.50	510.5	148.50
s8S	330.0	6.10	787.0	49.10
s8L	576.0	73.50	471.0	128.50

Table 11(a) Radiographic evaluation, group of iron (Fe)

Alloy	Evaluation
f1c	Moderate grain, moderate to heavy gas porosity; heavy copper segregation.
f1h	Moderate grain; heavy gas porosity; moderate to heavy copper segregation.
f2c	Moderate grain; moderate gas porosity; moderate to heavy copper segregation.
f2h	Moderate grain; moderate to heavy gas porosity; moderate to heavy copper segregation.
f3c	Fine grain, light to moderate porosity; heavy segregation.
f3h	Fine to moderate grain; light to moderate porosity near top half; moderate to heavy segregation.
f4c	Fine to moderate grain; heavy porosity; moderate gas cavities; moderate to heavy segregation.

Table 11(a) Continued.

Alloy	Evaluation
f4h	Fine to moderate grain; heavy gas porosity in top half of slice; moderate segregation.
f5c	Fine grain; moderate, dispersed porosity; heavy segregation.
f5h	Moderate grain; moderate, dispersed porosity; heavy, dispersed segregation.
f6c	Fine to moderate grain; heavy porosity; heavy segregation.
f6h	Fine to moderate grain; heavy porosity; moderate to heavy segregation.
f7c	Fine to moderate grain; moderate to heavy porosity in top half; moderate to heavy segregation.
f7h	Moderate grain; moderate porosity in top half; moderate segregation.
f8c	Fine grain; moderate to heavy porosity and gas cavities; heavy segregation.
f8h	Moderate grain, moderate to heavy porosity near top half.

Table 11(b) Radiographic evaluation, group of hydrogen (H)

Alloy	Evaluation
h1c	Fine grain; very light porosity; very coarse segregation.
h1h	Fine grain; very light porosity; very coarse segregation.
h2c	Very fine grain; heavy porosity and gas cavities; light segregation.
h2h	Very fine grain; very heavy porosity; light segregation.
h3c	Very fine grain; very heavy porosity and gas cavities; moderate to heavy segregation.
h3h	Very fine grain; very heavy porosity; light segregation.
h4c	Fine grain; very light porosity; heavy segregation.
h4h	Fine grain; very light porosity; heavy and well dispersed segregation.
h5c	Fine grain; heavy porosity and gas cavities; light to moderate segregation.
h5h	Fine grain; heavy porosity; light segregation.
h6c	Moderate grain; light porosity; moderate gas cavities; heavy segregation.
h6h	Moderate grain; very light porosity; moderate to heavy segregation.
h7c	Fine grain; very light porosity; some dense inclusions.
h7h	Fine grain; very light porosity; moderate to heavy inclusions; dispersed segregation.
h8c	Fine grain; very heavy gas porosity and gas cavities; moderate segregation.
h8h	Fine grain; heavy porosity; moderate to heavy segregation.

Table 11(c) Radiographic evaluation, group of strontium (Sr)

Alloy	Evaluation
s1c	Moderate to coarse grain; moderate to heavy gas porosity; light to moderate copper segregation.
s1h	Coarse grain; coarse gas porosity.
s2c	Fine grain; moderate to heavy gas porosity; heavy copper segregation.
s2h	Fine grain; heavy, coarse gas porosity; heavy copper segregation.
s3c	Coarse grain, light gas porosity; heavy copper segregation.
s3h	Coarse grain; light to moderate gas porosity; heavy copper segregation.
s4c	Fine grain; moderate gas porosity; light to moderate copper segregation.
s4h	Fine grain; heavy gas porosity; light to moderate to copper segregation.

Table 11(c) Continued.

Alloy	Evaluation
s5c	Fine grain; moderate to heavy porosity near top; heavy segregation.
s5h	Fine grain; heavy gas porosity; heavy segregation.
s6c	Moderate grain; heavy porosity and gas cavities; light dispersed segregation.
s6h	Moderate to coarse grain; heavy coarse porosity; light dispersed segregation.
s7c	Moderate grain; moderate porosity with gas cavities in centre; moderate segregation.
s7h	Moderate to coarse grain; heavy porosity in top half of slice; moderate segregation.
s8c	Moderate grain; moderate to heavy gas cavities near top half of slice; moderate segregation.
s8h	Coarse grain; moderate porosity; moderate segregation.

minimum hydrogen level used with the highest strontium concentration (300 p.p.m) is about 0.25 ml $100\,g^{-1}$ Al. Thus, it is somewhat difficult to determine the role of strontium alone from a direct comparison with other plates (having hydrogen contents < 0.25 ml $100\,g^{-1}$ Al). Strontium contributes considerably to both porosity volume fraction and pore size [19], as exemplified in Fig. 8.

Microstructural observations were made on polished, unetched surfaces of the samples corresponding to small (S), medium (M) and large (L) shown in Fig. 1 (and denoted by the letters S, M, L accordingly, in the alloy sample designations given in the tables). Fig. 9a, b shows the effect of soldification time for a degassed alloy (in the absence of Sr or grain

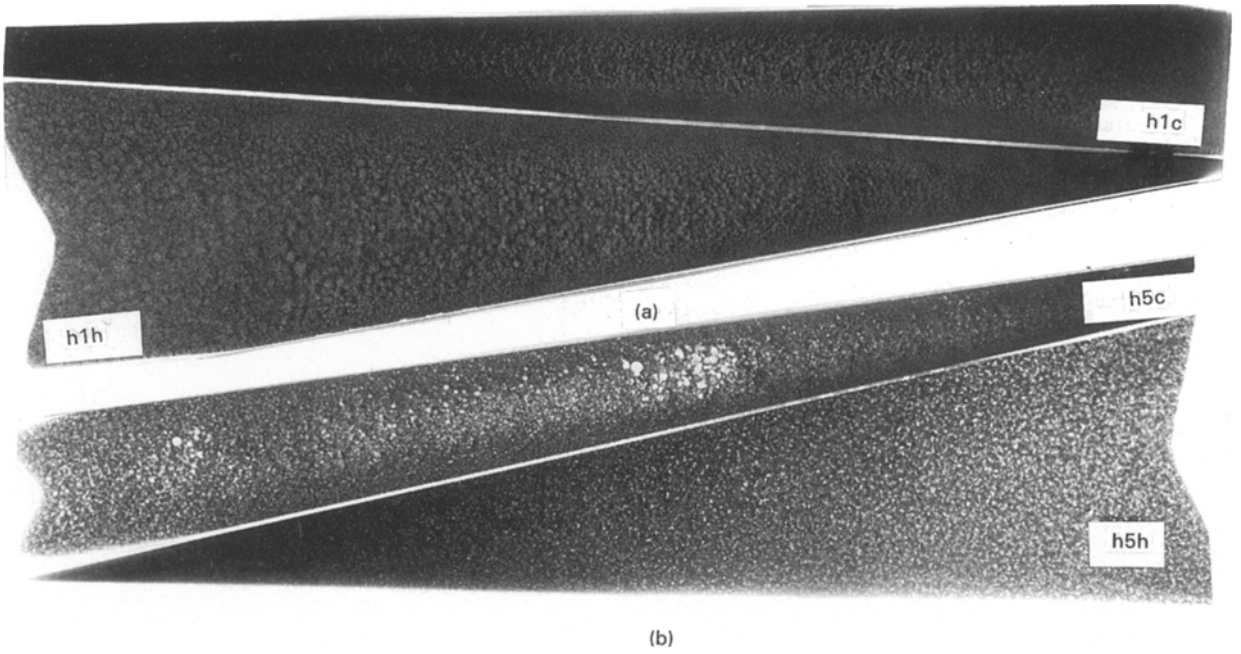

Figure 6 Radiographs corresponding to (a) h1, and (b) h5 alloys.

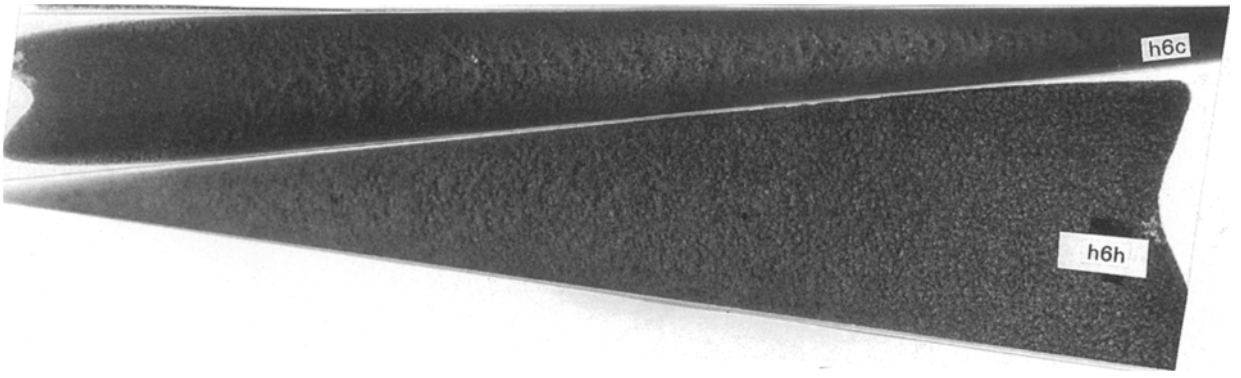

Figure 7 Radiographs corresponding to h6 alloy.

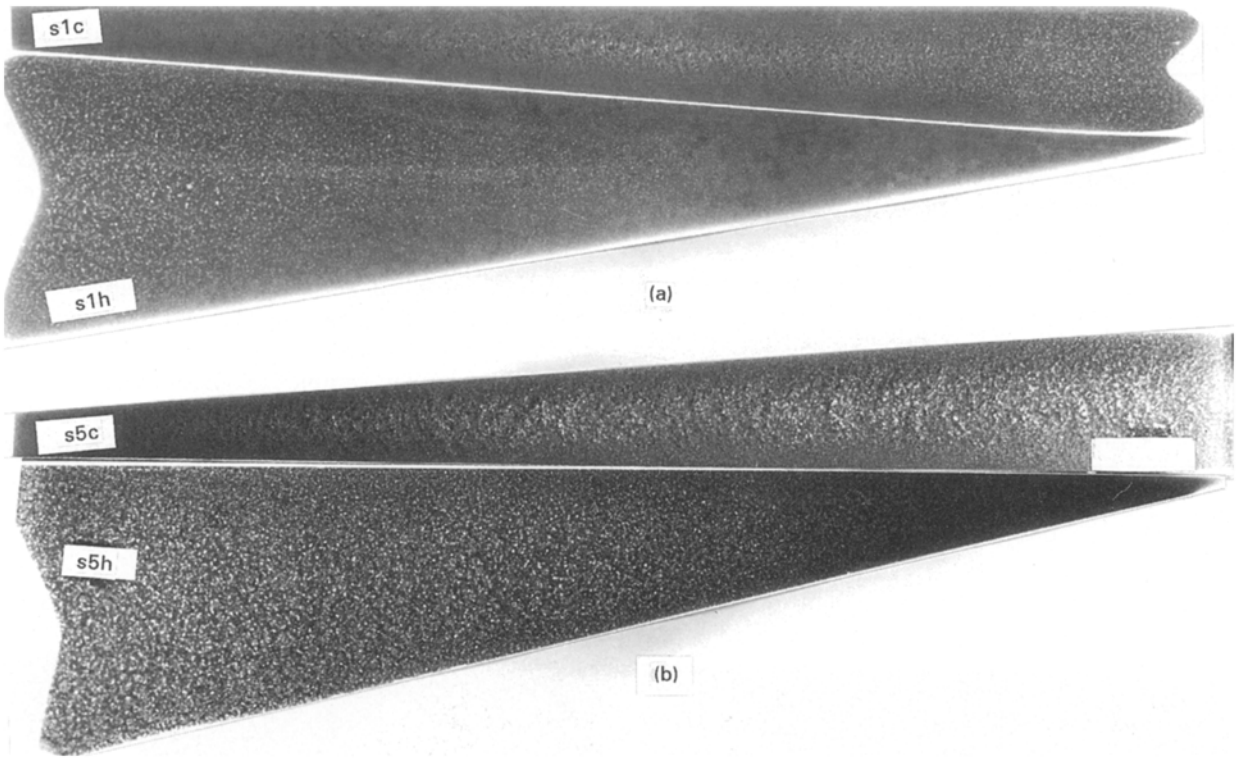

Figure 8 Radiographs corresponding to (a) s1, and (b) s5 alloys.

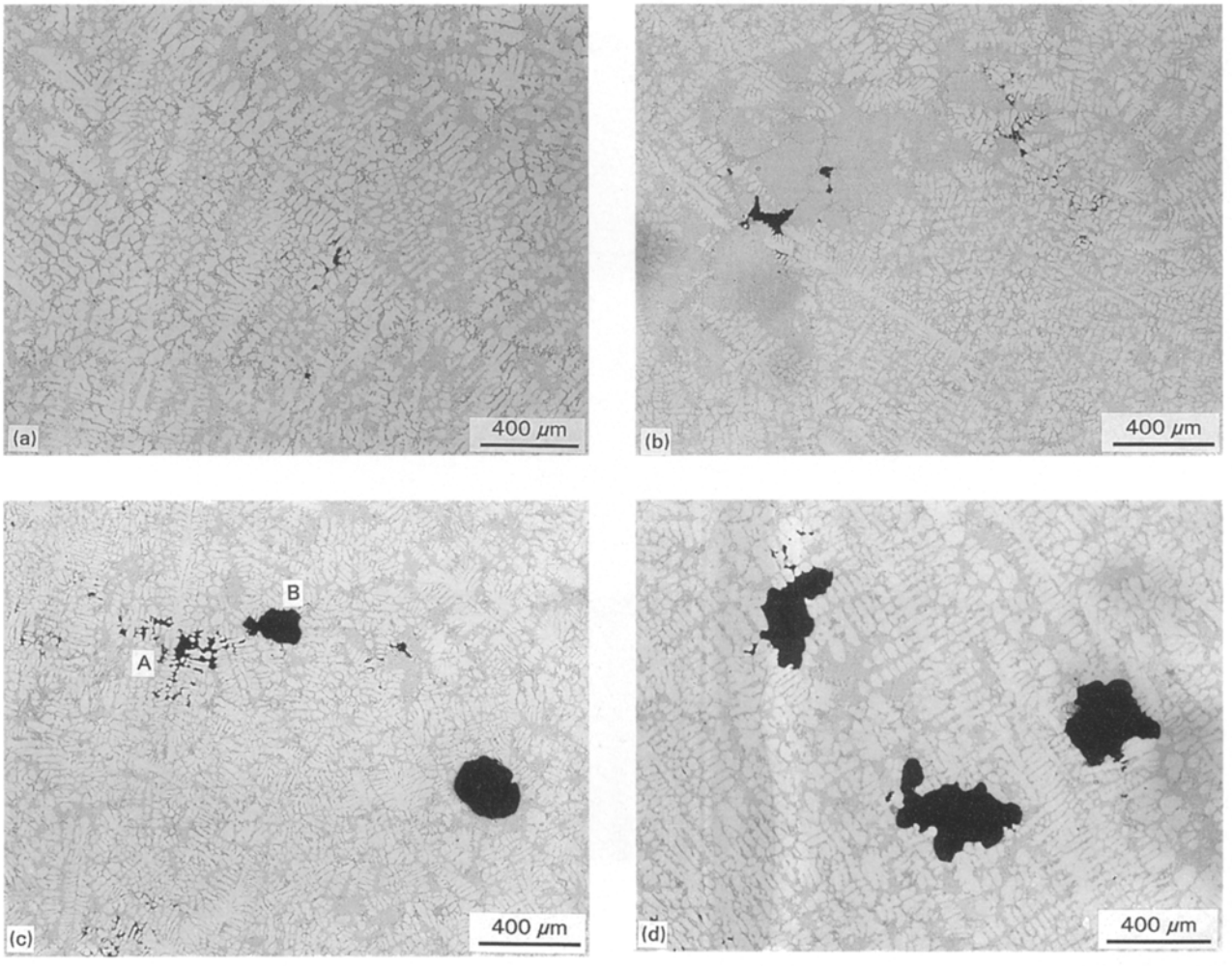

Figure 9 Optical microstructure of pores viewed in (a) h1S, (b) h1L, (c) h5S, and (d) h5L samples.

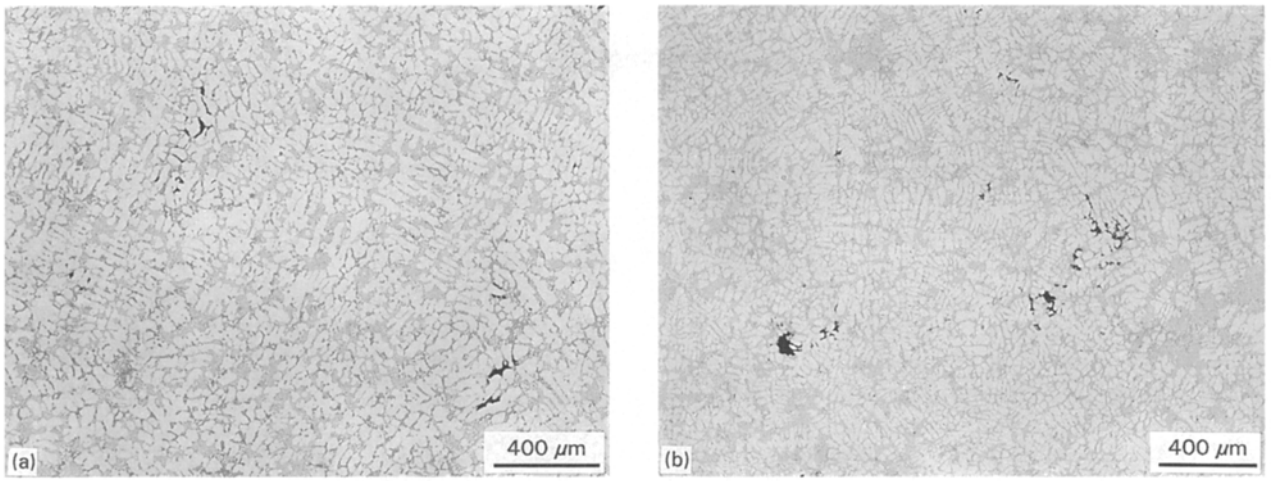

Figure 10 Optical microstructure of pores viewed in (a) h6S, and (b) h6L samples.

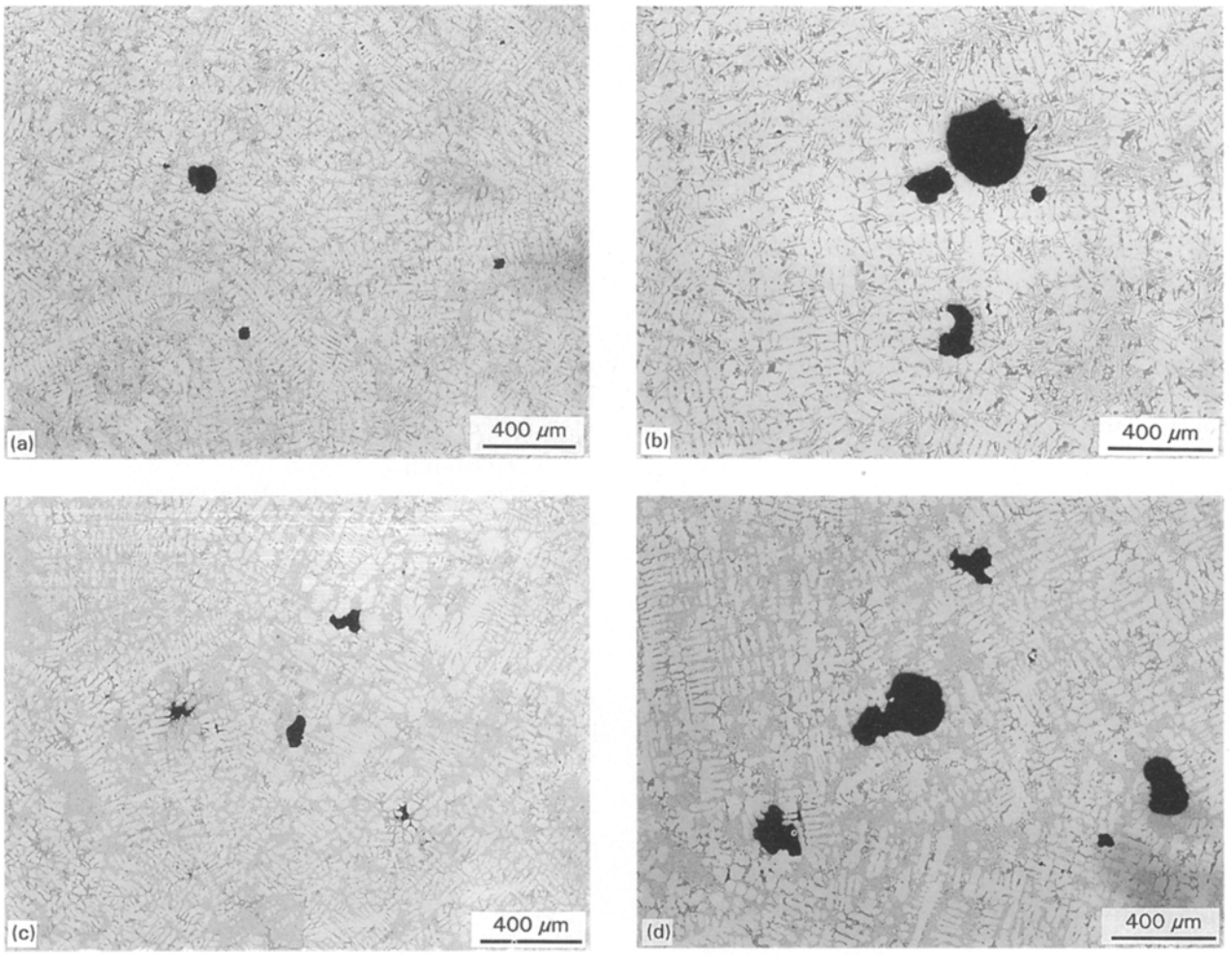

Figure 11 Optical microstructure of pores viewed in (a) s1S, (b) s1L, (c) s5S, and (d) s5L samples.

refiner addition). While it was rather difficult to observe any pores in the small sample, Fig. 9a, a few irregular/elongated pores could be observed for the large sample, Fig. 9b. The corresponding per cent surface porosities for the S and L samples are 0.06 and 0.08%, respectively (see Table VII).

The pores in samples containing 0.57 ml H 100 g^{-1} i.e. h5 alloy revealed two distinct morphologies, namely irregular and rounded, depending on the local solidification time. The length of the irregular pores (marked A in Fig. 9c) is approximately the same as the dendrite arm spacing, or slightly more. Such pores are normally termed "shrinkage pores", and are caused by an insufficient flow of liquid metal to fill the spaces between the dendrites, especially in the case of a cold mould. The fact that the volume fraction of this category of porosity is very low is attributed to the high silicon content (9 wt %) of the alloy, which considerably improves its fluidity [16]. The gas pores are characterized by their rounded form (marked B in

Fig. 9c). Increasing the solidification time leads to a rapid increase in the pore size as demonstrated in Fig. 9d.

Grain refining has an opposite effect to that of hydrogen. Addition of TiB_2 (as 0.02 wt % Ti) to the h1 alloy did not cause a noticeable effect at either low (Fig. 10a) or high (Fig. 10b) solidification time. Table VII shows the respective surface porosities to be 0.14 and 0.22%.

In unmodified alloys, e.g. s1, pores are mainly due to gas as inferred by their rounded shape, Fig. 11a, with a significant increase in their size for high solidification times, Fig. 11b. In the alloys with 300 p.p.m. Sr, the number of pores increases, as illustrated in Fig. 11c. The pores, however, are of the same size as those shown in Fig. 11a, and evenly distributed throughout the microstructure without forming a continuous network. A similar observation was made for the large sample, as seen in Fig. 11d.

4. Conclusions

1. Accurate measurements of porosity using image analysis need careful adjustment of optical parameters, namely focus, illumination and grey level, and a careful selection of the number of fields of measurement required to correctly represent the sample surface.

2. Not all alloying elements contribute to porosity formation in Al–Si–Cu base systems. A number of these elements, e.g. magnesium, titanium and phosphorus, result in reducing both pore size and density.

3. Hydrogen is the strongest element influencing porosity formation. Its effect is reinforced either by the addition of strontium, or by increasing the solidification time, or both.

4. Grain refining reduces pore density and size, and results in a fine dispersion of the pores throughout the alloy matrix.

Acknowledgements

The authors wish to thank Mr. G. Hayes of Kingston Research and Development Centre, Alcan International Limited, for carrying out the radiographic analysis, and KB Alloys, Inc., Robards, KY, USA, for supplying the master alloys used in the present work. Financial support received from the Natural Sciences and Engineering Research Council of Canada is gratefully acknowledged.

References

1. D. E. J. TALBOT, *Int. Metall. Rev.* **20** (1975) 166.
2. R. D. PEHLKE, in "Foundry Processes: Their Chemistry and Physics," edited by G. Katz and C. F. Landfeld, General Motors Reseach Laboratories, Warren, Michigan, September 1986 (Plenum Press, New York, 1988) pp. 427–445.
3. Q. T. FANG, P. N. ANYALEBECHI and D. A. GRANGER, *Light Metals* (The Minerals, Metals and Materials Society, Warrendale, PA, 1988) 977.
4. D. E. J. TALBOT and D. A. GRANGER, *J. Inst. Metals* **92** (1963–64) 290.
5. R. L. COBLE and M. C. FLEMINGS, *Met. Trans. A* **2** (1971) 409.
6. H. FREDRIKSSON and I. SVENSSON, *Met. Trans. B* **7** (1976) 599.
7. P. M. THOMAS and J. E. GRUZLESKI, *ibid.* **9** (1978) 139.
8. S. N. TIWARI and J. BEECH, *Met. Sci.* **12** (1978) 356.
9. J. E. GRUZLESKI, P. M. THOMAS and R. A. ENTWHISTLE, *Brit Foundryman* **71** (1978) 69.
10. F. WEINBERG and D. A. HIRSCHFELD, *Met. Sci.* **13** (1979) 335.
11. M. ABBAS, G. R. ST-PIERRE and C. E. MOBLEY, *AFS Trans.* **94** (1986) 47.
12. T. S. PIWONKA and M. C. FLEMINGS, *Trans. Met. Soc. AIME* **236** (1966) 1157.
13. J. CAMPBELL, *Cast. Met. Res. J.* **4** (1969) 1.
14. *Idem, Trans. Met. Soc. AIME* **239** (1967) 138.
15. *Idem*, "The Solidification of Metals", Publication 110 (Iron and Steel Institute, London, 1967) p. 18.
16. F. H. SAMUEL, H. LIU and A. M. SAMUEL, *Metall. Trans. A* **24** (1993) 1631.
17. R. GRUGEL and W. KURZ, *ibid.* **18** (1987) 1137.
18. S. GOWRI and F. H. SAMUEL, *ibid.* **25** (1994) 437.
19. A. M. SAMUEL and F. H. SAMUEL, *J. Mater. Sci.* **30** (1995) 4823.
20. Q. T. FANG and D. A. GRANGER, *AFS Trans.* **98** (1990) 897.

Received 6 March
and accepted 2 May 1995